Radio Science, Volume 4, Number 9, pages 771–780, September 1969

Dynamo currents, winds, and electric fields

S. Matsushita

High Altitude Observatory, National Center for Atmospheric Research
Boulder, Colorado 80302

(Received May 6, 1969.)

After a brief presentation of S_q and L electric current systems deduced from geomagnetic data, electric conductivities and wind models in the dynamo region are discussed. It is then shown that the solar negative-mode thermal diurnal tide and the lunar semidiurnal gravitational tide having a phase shift with altitudes produce the best fit S_q and L current systems, respectively. Distributions of electrostatic fields are computed, and electromagnetic drift speeds in the ionospheric F region are also examined. These calculated values agree well with observed results.

1. DEDUCED DYNAMO CURRENT SYSTEMS

Methods of deduction of dynamo currents and the remaining problems, particularly the S_q and L current systems and the equatorial electrojet, were reviewed by *Matsushita* [1967*a*, *b*] and *Onwumechilli* [1967]. Since the electric conductivity in the dynamo region (90–150 km altitude) is very low at night on geomagnetically quiet days, the dynamo currents on quiet nights may be almost zero. On the basis of this idea, *Matsushita* [1968] obtained computer-plotted S_q and luni-solar current systems for three seasons and the yearly average from his previously obtained current systems [*Matsushita*, 1967*b*] by shifting the base line. Figure 1 shows S_q current systems deduced in this way.

To obtain better luni-solar current systems than those deduced by using a relatively simple adjustment parameter [*Matsushita*, 1968, Figure 11], more realistic parameters are estimated from global $(f_0E)^2$ distributions in equinoctial and solstitial months during moderate sunspot periods. Figure 2 presents distributions of the parameter with respect to the dip latitude and the local time for the equinoctial and the June solstitial months; a reversal of the hemisphere for the June solstitial months is assumed to be the distribution for the December solstitial months. Multiplying the L current systems of a mean lunation [*Matsushita*, 1967*b*] by these parameters produces the L current systems for a new moon or the luni-solar current systems exhibited in Figure 3. The total current intensities are compared in Table 1.

The deduced S_q and L current systems clearly show the electrojet over the magnetic equatorial zone. These equatorial electrojets in the dynamo region were further confirmed by recent rocket observations (S_q by *Davis et al.* [1967], *Maynard* [1967], and *Sastry* [1968]; L by *Maynard* [1967]). In section 4, S_q and L current systems with the electrojet, computed from estimated electric conductivities and wind models, are compared with these deduced current systems.

2. ELECTRIC CONDUCTIVITY MODEL

By assuming that the physical quantities of the ionosphere are the same everywhere along the dip equator except for the differences arising from the asymmetry of the earth's permanent magnetic field, the cross-sectional profiles of the effective conductivity (hence the electrojet), were determined by *Sugiura and Cain* [1966] for different longitudes, particularly 80°E for India and 280°E for Peru. *Price* [1968, 1969] examined the applicability of the layer conductivities in the two-dimensional treatment of the dynamo theory of S_q. Calculations with a simple three-dimensional model suggest that the currents arising from wind-induced electromotive forces are nearly horizontal throughout the dynamo layer, so that the two-dimensional equations involving the layer conductivities can be used. However, the assumption that the horizontal current density is nondivergent and that consequently a current function can be found has been shown to be quite untrue.

For the purpose of obtaining total electric field distributions calculated from the deduced current sys-

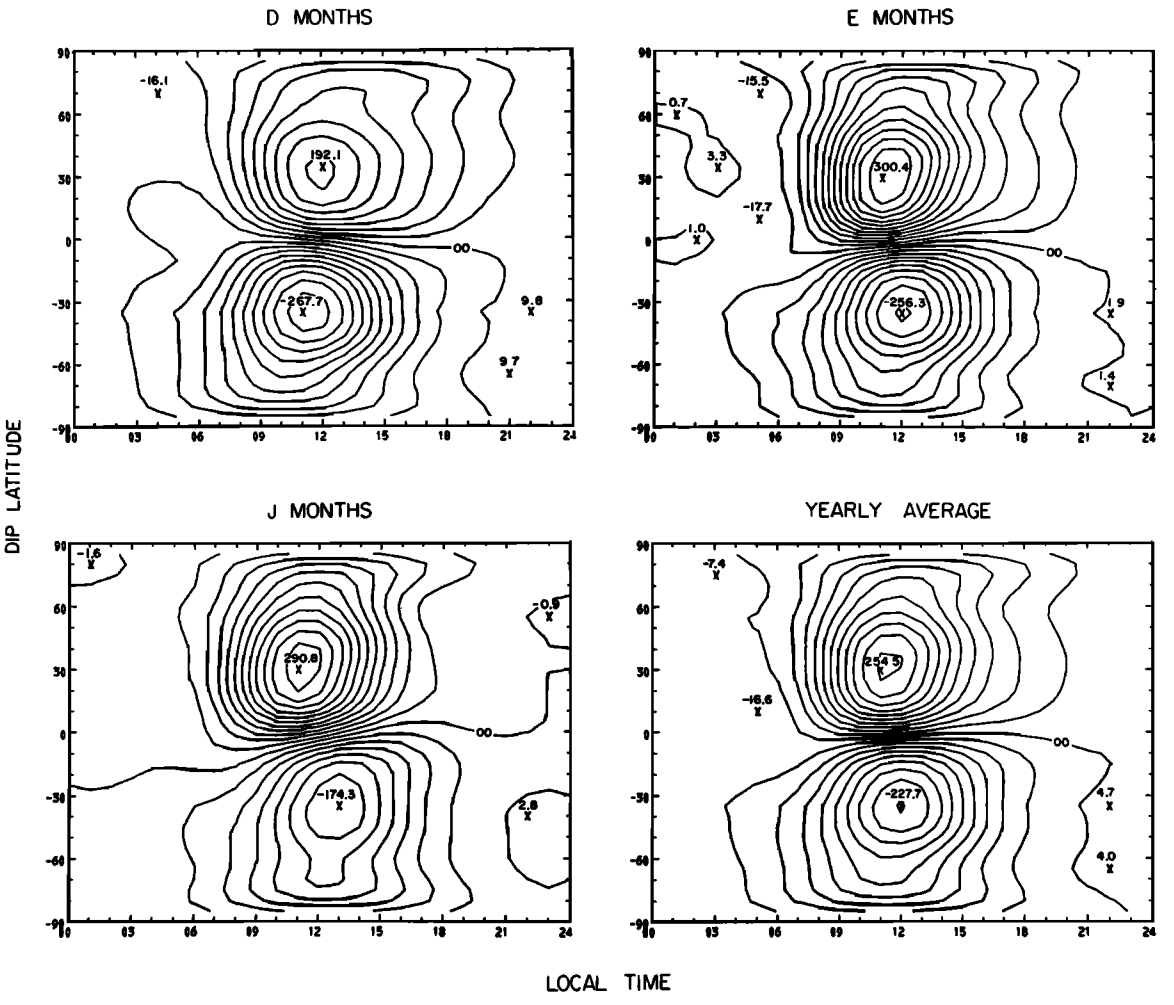

Fig. 1. Computer-plotted external S_q current systems for December solstitial, equinoctial, and June solstitial seasons and the yearly average during the IGY (1958) when the current intensity at the midnight is zero. The current intensity between two consecutive lines is 25×10^3 amp, and the numbers near the cross marks indicate the total current intensities of vortices in units of 10^3 amp [*Matsushita*, 1968].

tem and of computing current systems with wind models, a simple but reasonable model of the electric conductivity is needed. From the COSPAR-1965 atmosphere model, collision frequencies were computed by using the equations derived by *Nicolet* [1953] for the electron-ion collision frequency and by *Dalgarno* [1961] for the electron-neutral and the ion-neutral collision frequencies. Obtained height-integrated anisotropic electric conductivity distributions for two seasons during the IGY are shown in Figure 4. The conductivity distribution for December solstitial months can be approximated by the reversal of the hemisphere in the distribution for June solstitial months. The height-integrated conductivities for moderate sunspot periods are assumed to be 1/1.3 of the values for the IGY indicated in Figure 4. These conductivities and the L current system exhibited in Figure 3 give the total electric field (dynamo and electrostatic fields) for the L; the S_q current system in Figure 1 and the conductivity in Figure 4 present the total electric field for the S_q. These total field distributions for the S_q and L were illustrated by *Matsushita and Reddy* [1968]: the total electric field in low latitudes is a few mvolt/m for the S_q and a few tenths of mvolt/m for the L. The very small values of the field over the equator indicate that the estimated conductivity is probably too large for the equator.

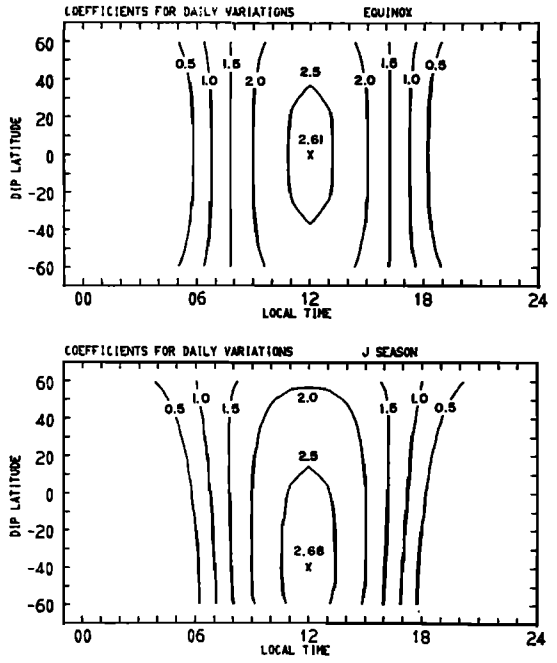

Fig. 2. Adjustment parameter distributions in two seasons.

To compute current systems, a slightly modified conductivity model for equinoctial months during moderate sunspot periods was obtained by *Tarpley* [1969]. The maximum value of σ_1 (Pedersen conductivity) in middle latitudes at noon is 3.1×10^{-15} emu at 127 km altitude and that of σ_2 (Hall conductivity) is 4.5×10^{-15} emu at 117 km. The tensor components of the height-integrated conductivity at noon are shown in Table 2. For the daily variation of the conductivity

$$\sum = \sum_{\text{noon}} \cos^{1/2} t$$

is adopted, and the conductivity during the period 1830 through 0530 LT is assumed to be constant and equal to 1/30 of the noon value. For details of temporal, latitudinal, and height distributions of the conductivity, refer to *Tarpley* [1969]. Computed results of the current systems using this conductivity model are presented in section 4.

3. WIND MODEL

We have recently gained a large amount of knowledge about the movements of ionospheric irregularities and upper atmospheric winds by various observational techniques and extensive theoretical estimations [e.g., *Hines*, 1966; *Woodrum and Justus*, 1968; *Kent and Wright*, 1968]. Data from a new meteor-wind observation system in France for 80–110 km altitudes (M. A. Spizzichino, private communication) have been processed by power spectral analysis to assess prevailing and tidal components and to analyze the residual nontidal contributions. The major component is semidiurnal, with a vertical wavelength greater than 50 km and an amplitude of 10–70 m/sec. A downward phase velocity of 5–10 km/hr is largely due to the semidiurnal component. Similar results for 90–130 km altitudes at night have also been obtained by observations of chemiluminous trails released by rockets and gun-launched projectiles [e.g., *Wright et al.*, 1967; *Bedinger et al.*, 1968].

A statistical analysis of seventy midlatitude vapor trails between 90 and 150 km altitude made by *Rosenberg* [1968] showed not only a consistent zonal flow to the east below 100 km, but also mean values of total velocity of 50 to 70 m/sec and mean shears of 0.02 to 0.004 m/s/m, varying with height. One full rotation occurs between 90 and 110 km and another occurs between 105 and 150 km. The height-integrated current intensity caused by the dynamo action of this type of rotated wind will be very small.

Those areas of wind measurements in which adequate data are not yet available include vertical winds, daytime winds above 110 km, and horizontally spaced winds to permit convergence estimates. Thus it is still difficult from observations to know a detailed global picture of the wind system responsible for dynamo currents. Also estimations of the wind patterns from dynamo currents and given conductiv-

TABLE 1. Total current intensities of L current systems ($\times 10^3$ amp)

Season:	D		E		J		Average	
Hemisphere:	N	S	N	S	N	S	N	S
Mean lunation	3.77	−5.54	5.09	−5.09	4.59	−2.68	4.16	−4.11
Luni-solar (before 1200)	6.15	−10.74	10.24	−10.24	9.54	−4.03	8.34	−8.19
(after 1200)	−9.00	10.82	−11.77	11.77	−8.90	6.89	−9.47	9.51

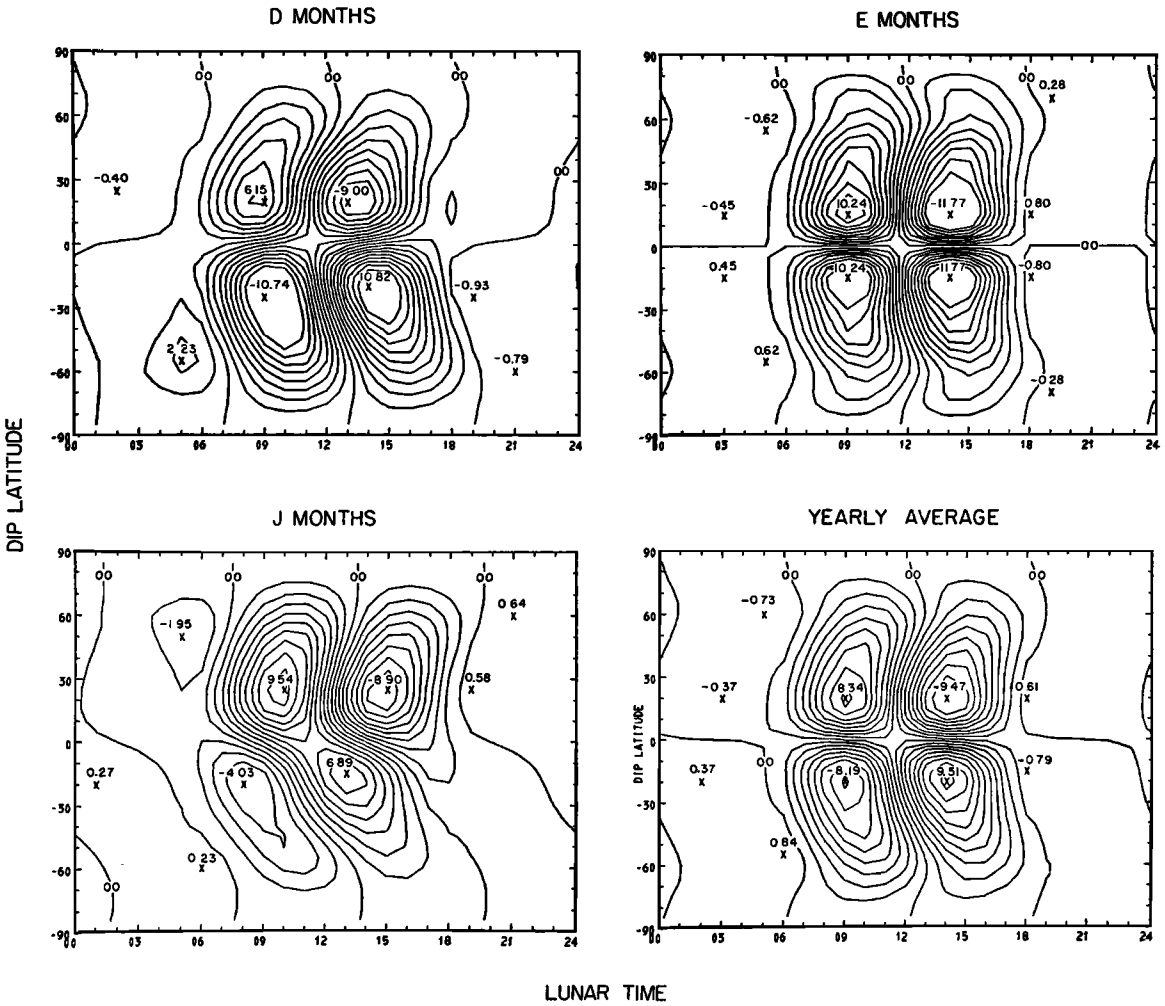

Fig. 3. Estimated L current for a new moon (or luni-solar current system) during three seasons and the yearly average (moderate sunspot period). The current intensity between two consecutive lines is 10^3 amp.

ity models are an interesting practice, but they are not always very meaningful because of the phase shift [e.g., *Maeda and Fujiwara,* 1967]. One possible way to attack the problem of explaining dynamo currents is (1) to assume a reasonable wind model based on currently available knowledge of the upper atmospheric winds, (2) to calculate current systems from the wind model and a reasonable conductivity distribution, and (3) to compare the obtained current systems with the ones estimated from geomagnetic variations. If the calculated current systems are similar to the estimated ones, the assumed wind model may give a hint as to the actual wind pattern.

On the basis of this idea, *Maeda and Murata* [1968] and *Maeda* [1968] assumed meridional and zonal wind systems and obtained current systems for each of the wind systems. Also, to explain the S_q and solar flare current systems, *Greenfield and Venkateswaran* [1968] assumed various periodic and nonperiodic wind models and computed current systems for each model. One common difficulty with these results was that the computed current focus appeared at places greatly different from the estimated one.

To have theoretical wind models, tidal theories need to be examined. The latitudinal structure of a tidal mode can be determined by the solution of Laplace's tidal equation, which has the Hough function $\Theta_{m,s}$ and its associated eigenvalue, namely, the equivalent depth $h_{m,s}$ for the tidal mode (m, s), where m denotes the longitudinal wave number ($m = 1$ for diurnal and $m = 2$ for semidiurnal tides) and $|s| - m$ is the number of modes in the Hough func-

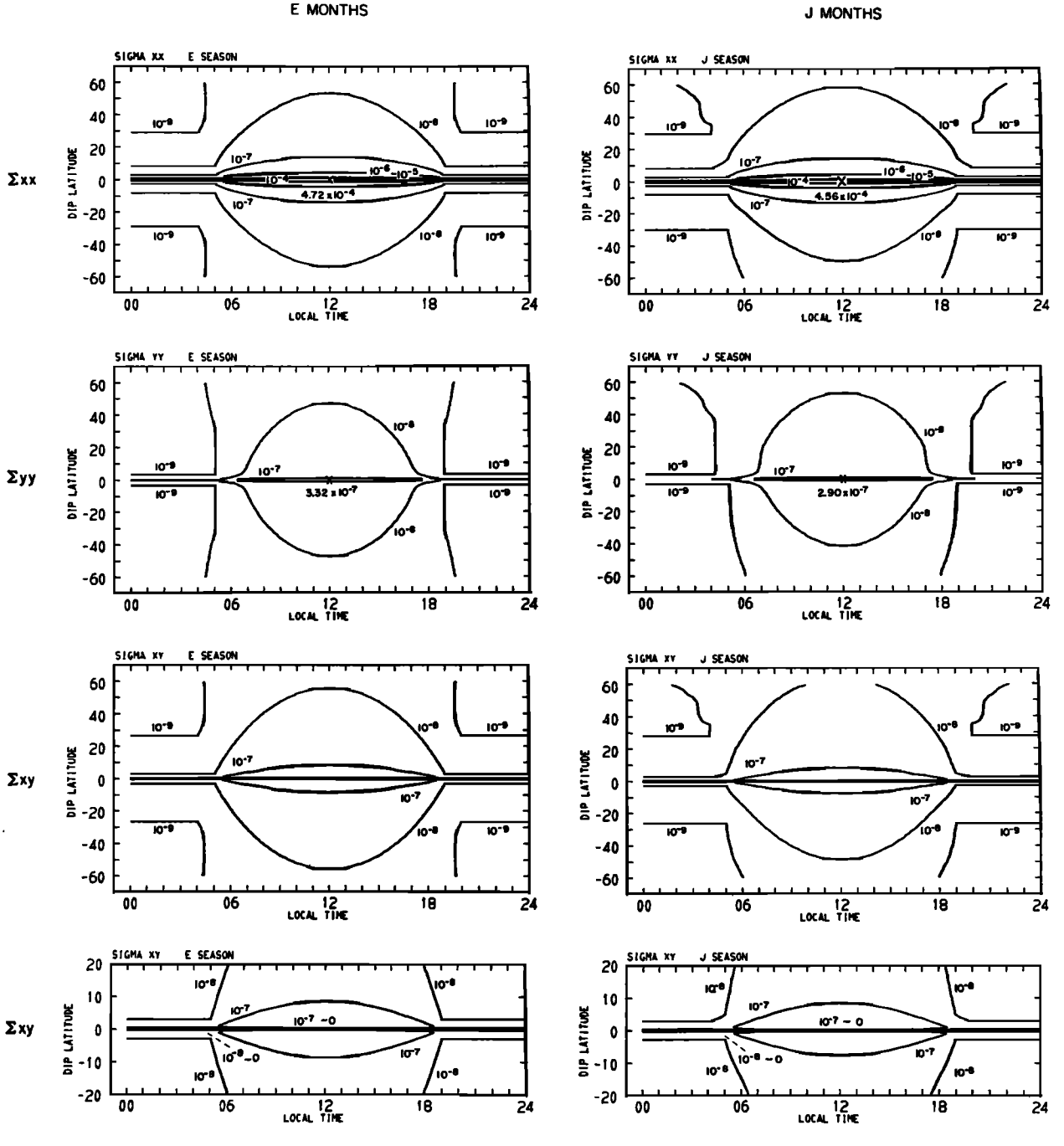

Fig. 4. Distributions of height-integrated anisotropic electric conductivities Σ_{xx}, Σ_{yy}, and Σ_{xy} with respect to the dip latitude and the local time for the IGY period. The unit is emu. The bottom two diagrams present Σ_{xy} distributions enlarged for low latitudes.

TABLE 2. Height-integrated conductivities in different latitudes at noon

Latitude, deg	Σ_{xx}, emu	Σ_{xy}, emu	Σ_{yy}, emu
0	1.07×10^{-4}	0	2.50×10^{-7}
1	1.03×10^{-5}	5.88×10^{-7}	5.28×10^{-8}
2	2.83×10^{-6}	3.31×10^{-7}	2.58×10^{-8}
3	1.28×10^{-6}	2.25×10^{-7}	1.95×10^{-8}
6	3.24×10^{-7}	1.12×10^{-7}	1.51×10^{-8}
9	1.45×10^{-7}	7.30×10^{-8}	1.38×10^{-8}
12	8.28×10^{-8}	5.34×10^{-8}	1.30×10^{-8}
15	5.40×10^{-8}	4.15×10^{-8}	1.22×10^{-8}
21	2.89×10^{-8}	2.79×10^{-8}	1.08×10^{-8}
30	1.55×10^{-8}	1.78×10^{-8}	8.90×10^{-9}
45	8.14×10^{-9}	1.03×10^{-8}	6.52×10^{-9}
60	5.41×10^{-9}	6.91×10^{-9}	4.99×10^{-9}
75	4.27×10^{-9}	5.38×10^{-9}	4.19×10^{-9}
90	4.05×10^{-9}	5.12×10^{-9}	4.05×10^{-9}

tion between the poles. The Hough function and equivalent depths for the important tidal modes were calculated by several workers: by *Kato* [1966*a*, *b*] and *Lindzen* [1966, 1967] for the solar diurnal modes, by *Siebert* [1961] for the solar semidiurnal modes, and by *Sawada* [1954, 1956] for the lunar tide.

Tarpley [1969] has examined various modes of solar and lunar tides together with nonperiodic winds for their effects on the production of dynamo currents. Among solar semidiurnal tides, (2, 2) and (2, 4) modes, and solar diurnal tides, (1, 3) and (1, −1) modes, the thermal-diurnal tide (1, −1) produces the best fit S_q current system. Since $h_{m,s}$ of this mode shows a negative value (−12.25 km), it is called a negative mode. When we use equations of the negative-mode thermal-diurnal tide (1, −1) shown by *Kato* [1966*a*], the adopted wind speeds in the dynamo region for the equinoctial months during a moderate sunspot period are

Southward:

$$u = A(\theta) \sin (\lambda + \gamma) \quad \text{m/sec} \tag{1a}$$

Eastward:

$$v = B(\theta) \sin (\lambda + \gamma + 90^\circ) \quad \text{m/sec} \tag{1b}$$

where θ is the colatitude, λ is the longitude, and $\gamma = 70°$. The amplitudes $A(\theta)$ and $B(\theta)$ are shown by

$$A(\theta) = 100\Phi_{uN}{}^{(-1)} \quad \text{m/sec}$$

$$B(\theta) = 100\Phi_{vN}{}^{(-1)} \quad \text{m/sec}$$

Here $\Phi_{uN}{}^{(-1)}$ and $\Phi_{vN}{}^{(-1)}$ are normalized values of $\Phi_u{}^{(-1)}$ and $\Phi_v{}^{(-1)}$, which are given with respect to θ in Figure 5. The mathematical forms of $\Phi_u{}^{(-1)}$ and $\Phi_v{}^{(-1)}$ refer to equations 3.23–3.25 in *Kato*'s paper [1966*a*].

A modified model for the solar (1, −1) mode suggested by *Tarpley* [1969] has the form

$$u = \frac{130}{0.25 - \cos^2\theta}\left(\frac{\partial}{\partial\theta} + 2\cot\theta\right)\Theta_{1,-1}(\theta) \cdot \sin(\lambda + \gamma) \quad \text{m/sec}$$

$$v = \frac{130}{0.25 - \cos^2\theta}\left(2\cos\theta\frac{\partial}{\partial\theta} + \operatorname{cosec}\theta\right)\Theta_{1,-1}(\theta) \cdot \sin(\lambda + \gamma + 90^\circ) \quad \text{m/sec} \tag{2}$$

where $\gamma = 250°$ and $\Theta_{1,-1}(\theta) = 0.7767P_1{}^1(\theta) + 0.5822P_3{}^1(\theta) + 0.0752P_5{}^1(\theta) + \cdots$. Here $P_n{}^m(\theta)$ are Schmidt functions. The wind distributions of these two models, particularly the latter one shown in Figure 6, present a surprising similarity to the diurnal wind distribution deduced from the dynamo theory of S_q for the rotating earth model by *Kato* [1956].

It must be noted that the solar (1, −1) mode is excited by a hypothetical *E*-region heat source, which is assumed constant with altitude and confined to a layer one scale height in thickness [*Kato*, 1966*b*].

Detailed theoretical work on the lunar atmospheric tide was conducted by *Sawada* [1954, 1956]. The lunar (2, 2) mode has the form

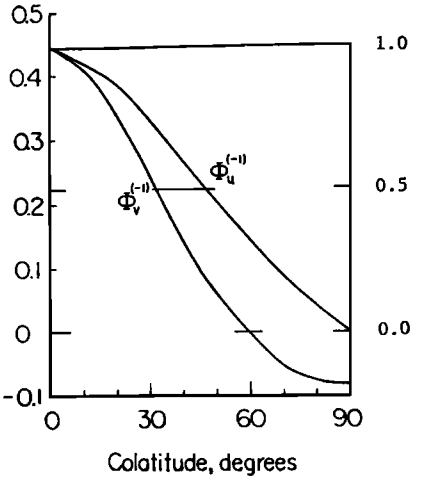

Fig. 5. $\Phi_u{}^{(-1)}$ and $\Phi_v{}^{(-1)}$ with respect to the colatitude given by *Kato* [1966*a*]. Read the right ordinate to find normalized values, $\Phi_{uN}{}^{(-1)}$ and $\Phi_{vN}{}^{(-1)}$.

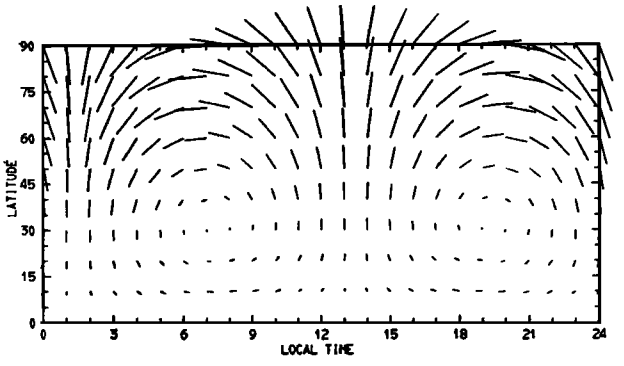

Fig. 6. Distribution of the wind vector by the negative-mode thermal diurnal tide represented by equation 2, which produces the best fit S_q current system. The lengths equal to 5° latitude correspond to 50-m/sec wind speed.

$$u = \frac{A(z)}{0.93 - \cos^2\theta}\left(\frac{\partial}{\partial\theta} + \frac{2\cot\theta}{0.96}\right)\Theta_{2,2}(\theta) \cdot \sin(2\lambda - 2\nu + kz + \gamma)$$

$$v = \frac{A(z)}{0.93 - \cos^2\theta}\left(\frac{\cos\theta}{0.96}\frac{\partial}{\partial\theta} + 2\operatorname{cosec}\theta\right)\Theta_{2,2}(\theta) \cdot \sin(2\lambda - 2\nu + kz + \gamma + 90°) \quad (3)$$

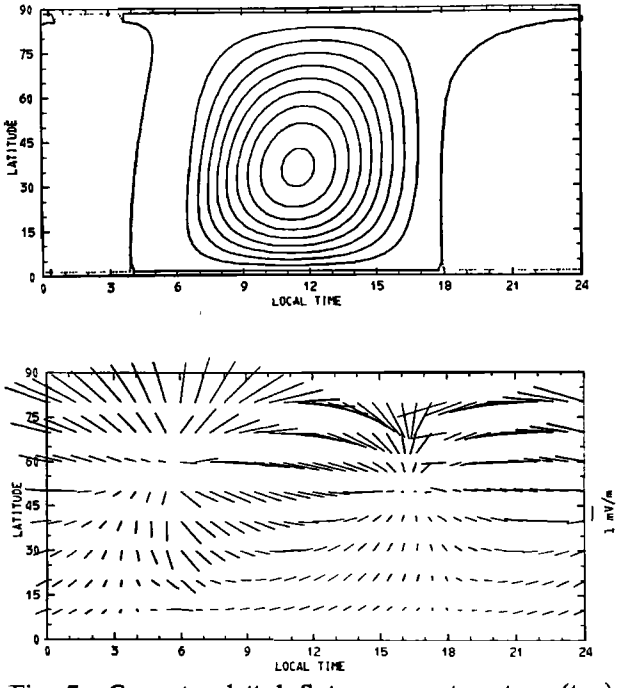

Fig. 7. Computer-plotted S_q-type current system (top) and electrostatic field distribution (bottom) calculated from the thermal tidal wind model shown by equation 1. The current intensity between two consecutive lines is 10^4 amp, and the circular current flow in the northern hemisphere is counterclockwise. The vector of the static field is plotted in 10° steps of latitude and longitude.

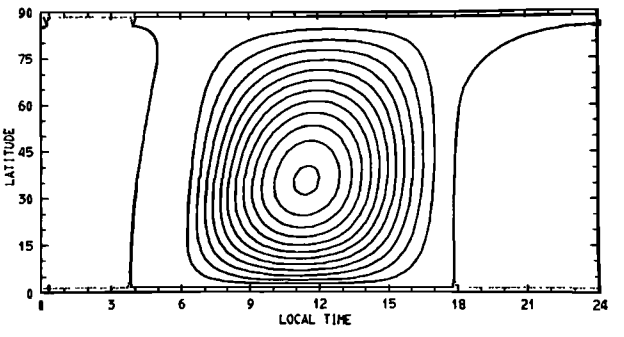

Fig. 8. Computer-plotted S_q-type current system calculated from the thermal tidal wind model shown by equation 2. The total current intensity is 121,850 amp and the position of the focus is at 36° latitude at 11.4 hour LT.

where τ is the lunar time taken to be zero at the lower transit, ν is the elongation of the moon or the age of the moon in hours, $\lambda = \tau + \nu$, and k is the vertical wave number. Here $\Theta_{2,2}(\theta) = 3.4641P_2^2(\theta) - 1.2987P_4^2(\theta) + 0.1736P_6^2(\theta) - \cdots$, and z is the vertical height above the lower boundary of the dynamo region, namely, 90 km in our model. In Sawada's wind fields for the altitude 90 km the phase constant γ lies in the range 210°–225°,

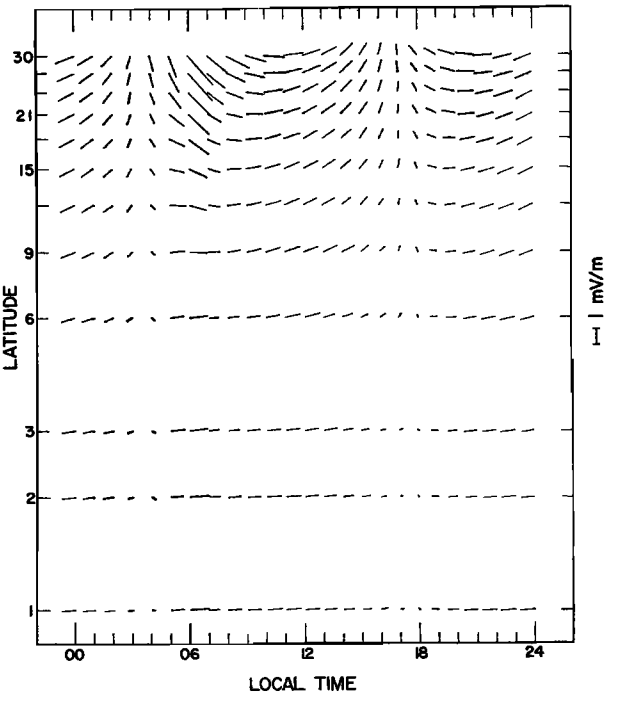

Fig. 9. Average S_q-type electrostatic field distribution expanded in low latitudes and plotted for each 10° step of longitude and each 3° step of latitude (also at 1° and 2° latitude) for the wind model shown by equation 2.

and the amplitude at latitude 30° lies in the range 2–8 m/sec, depending on the temperature profile of the lower atmosphere. Taking into consideration Sawada's theory, *Tarpley* [1969] adopted $A(z) = 7.5$ m/sec, $k = 4.25°$/km, and $\gamma = 228°$. This model of the lunar tide produces the best fit L current system, as shown in the next section.

4. OBTAINED DYNAMO CURRENTS AND ELECTROSTATIC FIELDS

The electric conductivity model mentioned in section 2 and the wind model represented by equations 1 and 2 in section 3 produce the current systems and electrostatic field distributions shown in Figure 7 and Figures 8 and 9, respectively. The general current pattern, the total current intensity, and the location of the current focus of both current systems present very reasonable results, comparing them with the deduced S_q current system shown in Figure 1 and bearing in mind that the current system in Figure 1 is for the active sunspot period (hence, large current intensity), whereas the current systems in Figures 7 and 8 are for the equinox during the moderate sunspot period. The phase constant γ in equation 2 can vary by ±45° about the value of 250° without greatly changing the current pattern.

It is clear in Figure 9 that the N-S component of the electrostatic field is very small in low latitudes, whereas the E-W field has a magnitude of near 1 mvolt/m and is directed eastward during daylight hours and westward at night. The change of direction occurs around the sunrise and sunset times.

The vertical electromagnetic drift speeds at 400 km altitude due to the coupling of the earth's main northward magnetic field and the computed E-W electrostatic field were calculated by *Tarpley* [1969]. The upward speed at noon is about 30 m/sec in the equatorial region and about 20 m/sec in middle latitudes, whereas the downward speed around midnight is about 30 m/sec in the equatorial region and about 15 m/sec in middle latitudes. In general, the results agree well with the observations of drift motions and estimations of the static field made by radio waves at Jicamarca, Peru [*Balsley,* 1969], and by barium release experiments at Thumba, India (R. Lüst, private communication).

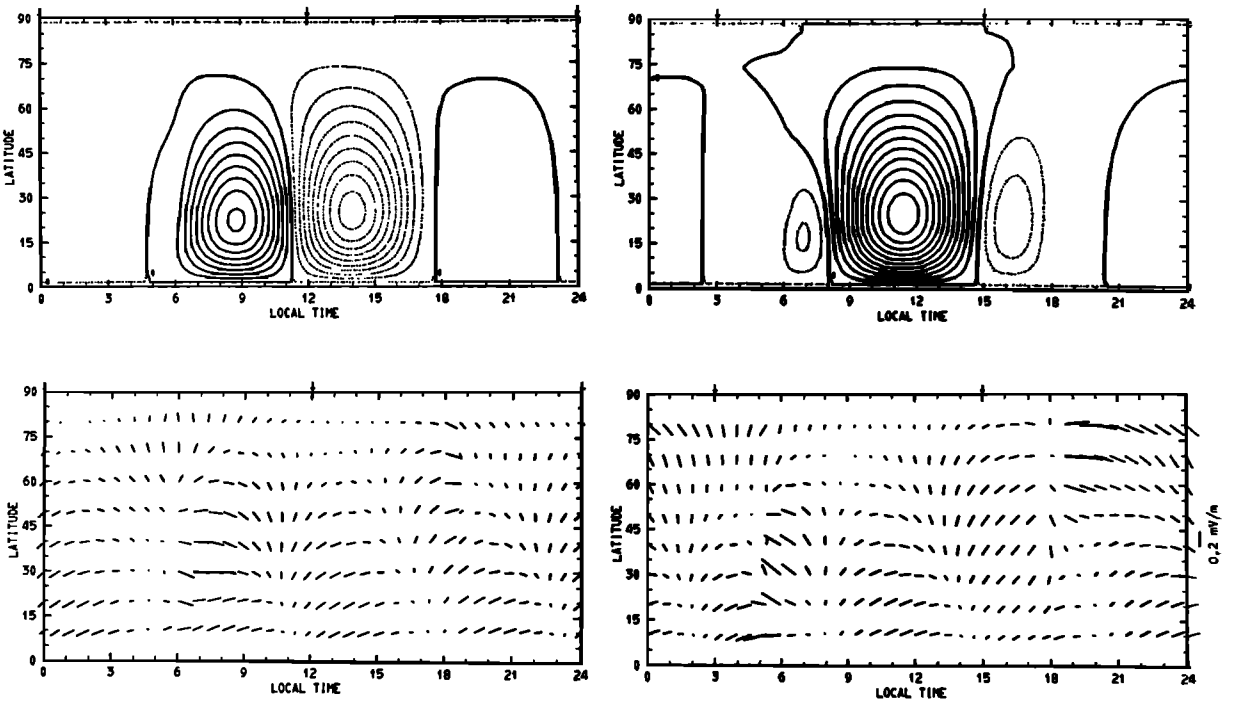

Fig. 10. Computer-plotted L-type current systems (top) and electrostatic field distributions (bottom) calculated from the semidiurnal lunar (2, 2) tidal wind model. The moon is over the 0- or 12-hour meridian in the left-hand diagrams, and over the 3- or 15-hour meridian in the right-hand diagrams. The current intensity between two consecutive lines is 10^3 amp, and the solid and dotted circular lines indicate counterclockwise and clockwise currents, respectively. The vector of the static field is plotted for each 10° step of latitude and longitude.

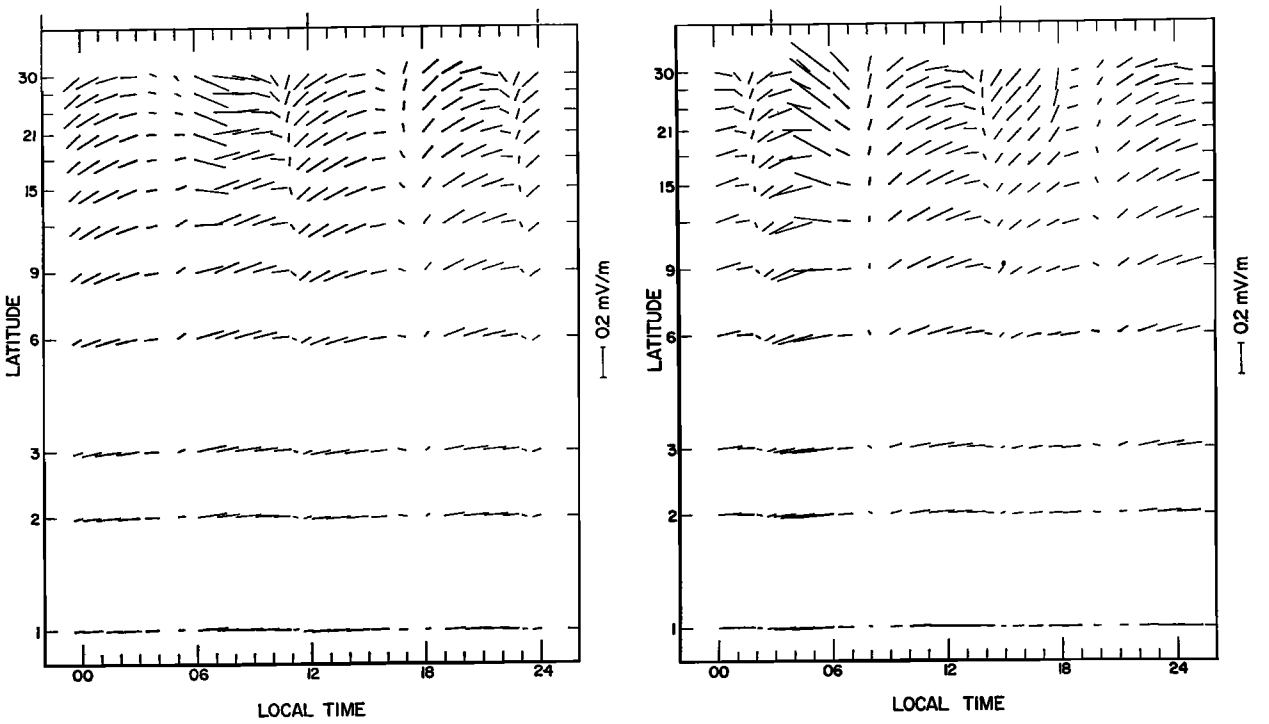

Fig. 11. Average L-type electrostatic field distribution expanded in low latitudes and plotted for each 10° step of longitude and each 3° step of latitude (also at 1° and 2° latitude). (*Left*) The moon is over the 0- or 12-hour meridian; (*right*) the moon, over the 3- or 15-hour meridian.

The current systems and the electrostatic field distributions for two lunar phases calculated from the conductivity and lunar tidal wind models discussed in the preceding sections are presented in Figure 10. The current system at the top left of Figure 10 is very similar to the yearly average L current pattern in Figure 3. The electrostatic field distributions for the two lunar phases expanded in low latitudes are shown in Figure 11. From these plots we see that the static field in the equatorial region is 0.2 mvolt/m or less.

In the same way as the solar variation, the vertical electromagnetic drift speeds for L at 400 km altitude can be computed. The maximum speed is about 5 m/sec in the equatorial region and a few meters per second in middle latitudes. Previously estimated electric fields and drift speeds due to L [*Matsushita*, 1967*a*, *b*] agree fairly well with these results.

This report provides only essential points and main results of dynamo currents, winds, and electric fields. For details of computations and discussions of the ionospheric wind dynamo, refer to *Tarpley* [1969] and his future full papers.

Acknowledgments. I wish to thank Professor S. Kato, Dr. J. D. Tarpley, Mrs. Mary Hilty, and Mrs. Harriet Bribitzer in my laboratory for their assistance.

REFERENCES

Balsley, B. B. (1969), Nighttime electric fields and vertical ionospheric drifts near the magnetic equator, *J. Geophys. Res., 74,* 1213–1217.

Bedinger, J. F., H. Knaflich, E. Manring, and D. Layzer (1968), Upper-atmosphere winds and their interpretation, *Planet. Space Sci., 16,* 159–193.

Dalgarno, A. (1961), Charged particles in the upper atmosphere, *Ann. Geophys., 17,* 16–49.

Davis, T. N., K. Burrows, and J. D. Stolarik (1967), A latitude survey of the equatorial electrojet with rocket-borne magnetometers, *J. Geophys. Res., 72,* 1845–1861.

Greenfield, S. M., and S. V. Venkateswaran (1968), The vertical structure of dynamo winds deduced from geomagnetic variations associated with solar flares, *Ann. Geophys., 24,* 665–672.

Hines, C. O. (1966), Diurnal tide in the upper atmosphere, *J. Geophys. Res., 71,* 1453–1459.

Kato, S. (1956), Horizontal wind systems in the ionospheric E region deduced from the dynamo theory of the geomagnetic S_q variation, 2, *J. Geomagn. Geoelec., Kyoto, 8,* 24–37.

Kato, S. (1966*a*), Diurnal atmospheric oscillation, 1, Eigenvalues and Hough functions, *J. Geophys. Res., 71,* 3201–3209.

Kato, S. (1966*b*), Diurnal atmospheric oscillation, 2, Thermal excitation in the upper atmosphere, *J. Geophys. Res., 71,* 3211–3214.

Kent, G. S., and R. W. H. Wright (1968), Movements of ionospheric irregularities and atmospheric winds, *J. Atmos. Terr. Phys., 30,* 657–691.

Lindzen, R. S. (1966), On the theory of the diurnal tide, *Mon. Weather Rev., 94,* 295–301.

Lindzen, R. S. (1967), Thermally driven diurnal tide in the atmosphere, *Quart. J. Roy. Meteorol. Soc., 93,* 18–42.

Maeda, H. (1968), Variation in geomagnetic field, *Space Sci. Rev., 8,* 555–590.

Maeda, H., and M. Fujiwara (1967), Lunar ionospheric winds deduced from the dynamo theory of geomagnetic variations, *J. Atmos. Terr. Phys., 29,* 917–936.

Maeda, H., and H. Murata (1968), Electric currents induced by nonperiodic winds in the ionosphere, *J. Geophys. Res., 73,* 1077–1092.

Matsushita, S. (1967*a*), Lunar tides in the ionosphere, *Handbuch der Physik, 49*(2), 547–602.

Matsushita, S. (1967*b*), Solar quiet and lunar daily variation fields, in *Physics of Geomagnetic Phenomena,* edited by S. Matsushita and W. H. Campbell, vol. 1, pp. 301–424, Academic Press, New York and London.

Matsushita, S. (1968), S_q and L current systems in the ionosphere, *Geophys. J., 15,* 109–125.

Matsushita, S., and C. A. Reddy (1968), Morphological behavior of blanketing sporadic E at middle latitudes, *Proc. Second E. Seminar, 1,* 1–3, 38.

Maynard, N. C. (1967), Measurements of ionospheric currents off the coast of Peru, *J. Geophys. Res., 72,* 1863–1875.

Nicolet, M. (1953), The collision frequency of electrons in the ionosphere, *J. Atmos. Terr. Phys., 3,* 200–211.

Onwumechilli, A. (1967), Geomagnetic variations in the equatorial zone, in *Physics of Geomagnetic Phenomena,* edited by S. Matsushita and W. H. Campbell, vol. 1, pp. 425–507, Academic Press, New York and London.

Price, A. T. (1968), Ionospheric conductivity and S_q variations, *Geophys. J., 15,* 93–102.

Price, A. T. (1969), Daily variations of the geomagnetic field, *Space Sci. Rev., 9*(2), 151–197.

Rosenberg, N. W. (1968), Dynamic model of ionospheric wind profiles, *J. Geophys. Res., 73,* 4965–4968.

Sastry, T. S. G. (1968), Quiet-day electrojet over Thumba, India, *J. Geophys. Res., 73,* 1789–1794.

Sawada, R. (1954), The atmospheric lunar tides, *Meteorol. Papers, 2*(3), New York University.

Sawada, R. (1956), The atmospheric lunar tides and the temperature profile in the upper atmosphere, *Geophys. Mag., Japan, 27,* 213–236.

Siebert, M. (1961), Atmospheric tides, *Advan. Geophys., 7,* 105–187.

Sugiura, M., and J. C. Cain (1966), A model equatorial electrojet, *J. Geophys. Res., 71,* 1869–1877.

Tarpley, J. D. (1969), The ionospheric wind dynamo, Ph.D. thesis, Astro-Geophysics Department, University of Colorado, Boulder.

Woodrum, A., and C. G. Justus (1968), Atmospheric tides in the height region 90 to 120 kilometers, *J. Geophys. Res., 73,* 467–478.

Wright, J. W., C. H. Murphy, and G. V. Bull (1967), Sporadic E and the wind structure of the E region, *J. Geophys. Res., 72,* 1443–1460.